IEEE Access
Multidisciplinary | Rapid Review | Open Access Journal

Received 17 July 2022, accepted 16 August 2022, date of publication 22 August 2022, date of current version 14 September 2022.

Digital Object Identifier 10.1109/ACCESS.2022.3200701

RESEARCH ARTICLE

Analytical Shielding Metrics-Based Shielding Configuration Guideline for ELF Magnetic Field Mitigation

KIBEOM KIM[1], MINSANG KIM[2], AND SANGWOOK PARK[2], (Member, IEEE)

[1]Alsemy, Gangnam-gu, Seoul 06154, Republic of Korea
[2]Division of Electronic and Electrical Engineering, College of Information and Communication Engineering, Daegu University, Gyeongsan 38453, Republic of Korea

Corresponding author: Sangwook Park (wave@daegu.ac.kr)

This work was supported by Korea Electric Power Corporation under Grant R21XO01-40.

ABSTRACT This paper presents a simple guideline for configuration of the shielding materials that mitigates the extremely low-frequency (ELF) magnetic fields generated by power facilities located close to our daily life activities. Generally, materials with high permeability and conductivity are used to mitigate the magnetic field; however, in the current source region, before passing through the shielding material, the magnetic field may be increased by the configuration of the shielding material. To assess the effect of the shielding configuration in the current source and shielding regions, metrics are newly introduced, which were obtained based on the analytical solution for infinite width shields. In addition, the analytical solution of the shielding pipe wrapping a current source was deduced by solving the cylindrical Helmholtz equation. The shielding pipe is an important factor that can bring about changes in the metrics introduced in this study. The simple shielding guidelines suggested from these analyses help determine strategies for designing shields that can mitigate the magnetic field in both the current source and shielding regions.

INDEX TERMS Extremely low frequency magnetic field, magnetic field mitigation, magnetic field shielding, power facilities.

I. INTRODUCTION

Awareness of the electromagnetic environment is continuously increasing. In particular, because power facilities generally deal with high-voltage- alternating current (AC) transmission,the extremely low-frequency (ELF) magnetic field generated by them is one of the main subjects of study [1]. The International Agency for Research on Cancer (IARC) classified the carcinogenicity of ELF as Group 2B (possibly carcinogenic to humans) in investigations into the causes of cancer [2], [3], [4], [5], [6], [7]. International Commission on non-Ionizing Radiation Protection (ICNIRP) establishes exposure limits for ELF magnetic fields [8]. Further, ELF has been reported to cause electromagnetic interference (EMI) problems in electronic devices [9], [10], which has the potential to cause catastrophic failures in power facility control and monitoring systems.

The associate editor coordinating the review of this manuscript and approving it for publication was Wenjie Feng.

In recent decades, many studies have been conducted on the technical possibility and effects of magnetic field suppression countermeasures applied near transmission or distribution lines [11]. These can be broadly classified into two categories: 1) creation of cancelling magnetic fields, such as those resulting from cable installation geometry [12], [13], [14] and passive shielding loops [15], [16]; 2) use of shielding materials, such as those with high permeability and conductivity [17], [18], [19], [20], and a suitable shielding material installation geometry [21], [22], [23].

The primary emphasis of methods using shielding materials focuses only on the mitigation of the magnetic field in the shielding region without considering the magnetic field in the current source region, which could affect the cable management operators or monitoring system. Shield effectiveness was introduced to evaluate the magnetic field shield, which is suitable for describing the degree of shielding from changes in the electrical properties of the shielding material, such as permeability and conductivity.

However, it is not an appropriate metric for shielding geometry, such as thickness, and cannot explain the effect of the shielding material, especially in the current source region.

The purpose of this paper is to suggest a simple shielding configuration guideline that covers both the source current and shielding regions. A theoretical analysis of infinite-width planar shields is presented in Section II. The metrics based on this analysis were defined by adding the reflection coefficient and geometrical shielding effectiveness. The reflection coefficient can explain the effect of shielding materials in the current source region, and the geometrical shielding effectiveness compensates for the weakness of the conventional shielding effectiveness, which cannot exactly describe the effect of the increase in the thickness of the shielding material. The solution of the Helmholtz equations in all regions is obtained by extending the approach of conventional research [13], without distinguishing whether the shielding material is a good conductor. In Section III, using these metrics, a detailed parametric analysis of the geometrical and electrical parameters of shielding materials is performed. Section IV describes the analytical approach used to calculate the magnetic field intensity generated by a current source wrapped with a shielding pipe. The shielding pipe mitigates the magnetic field incident on the shielding material, resulting in a change in the permeability of the shielding material. Section V presents an example of a shielding configuration that applies both the nonlinear B–H curve characteristic of shielding materials and the effect on the shielding pipe. Finally, simple shielding configuration guidelines are summarized in Section VI.

II. ANALYTIC SOLUTION AND METRICS FOR N-LAYER INFINITE PLANAR SHIELDS

A. ANALYTIC SOLUTION

The geometry of the shielding configuration is illustrated in Fig. 1. The current source in the current source region ($y < 0$) is located at and $y = y_s$, its magnitude is expressed as I_s. The current source is uniform and infinitely long in the z-direction. The regions from index 1 to N are occupied by shielding materials that have an infinite plane along the x-axis. The shielding material for each region is characterized by permittivity, ϵ_n, permeability, μ_n and conductivity, σ_n, where the subscript n indicates the index of the region. It is assumed that these parameters have a constant value. Unlike the region, which starts from index 0, the index of the interface starts from 1, and there is a total of N elements in each case. The y-position of each interface is denoted by T_n. The magnetic vector potential, $\boldsymbol{A}$, is useful for solving time-harmonic magnetic field. $\boldsymbol{A}$ is defined as the magnetic field $\boldsymbol{B} = \nabla \times \boldsymbol{A}$ and the electric field $\boldsymbol{E} = -\nabla\phi_e - \partial\boldsymbol{A}/\partial t$, where the scalar function, ϕ_e, denotes an arbitrary electric scalar potential which is a function of position, and t is a time [24]. The inhomogeneous Helmholtz equation for $\boldsymbol{A}$, which is a govern equation of the mathematical model, can

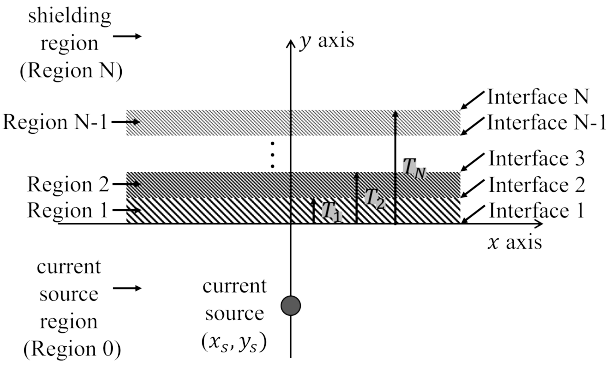

FIGURE 1. Basic shielding configuration. A horizontal current source is located under shielding materials with infinite width ($y_s < 0$).

be described as

$$\nabla^2\boldsymbol{A} + \omega^2\mu\epsilon\left(1 - j\frac{\sigma}{\omega\epsilon}\right)\boldsymbol{A} = \nabla\left\{\nabla\cdot\boldsymbol{A} + j\omega\mu\epsilon\left(1 - j\frac{\sigma}{\omega\epsilon}\right)\phi_e\right\} \quad (1)$$

where ω is the angular frequency. The curl of $\boldsymbol{A}$ was defined as $\boldsymbol{B}$, while the divergence of $\boldsymbol{A}$ which is independent of its curl has a liberty [25]. To get the greatest mathematical convenience for (1), let

$$\nabla\cdot\boldsymbol{A} = -j\omega\mu\epsilon\left(1 - j\frac{\sigma}{\omega\epsilon}\right)\phi_e \quad (2)$$

Substituting (2) into (1), (1) for $\boldsymbol{A}$ in each region n can be simplified as follows:

$$\nabla^2\boldsymbol{A_n} + p_n^2\boldsymbol{A_n} = 0 \quad (3)$$

A constant $p_n = \omega\sqrt{\mu_n\epsilon_n}\sqrt{1 - j\sigma_n/(\omega\epsilon_n)}$ is called complex propagation of the medium. $\boldsymbol{A_n}$ has only a z-component because the current source does not vary with z. Thus, $\boldsymbol{A}$ is expressed as a function of x and y and not of z.

$$\left(\frac{\partial^2}{\partial x^2} + \frac{\partial^2}{\partial y^2} + p_n^2\right)A_n(x, y) = 0 \quad (4)$$

The uniqueness theorem for time-harmonic electromagnetic waves states that the solution satisfies Maxwell's equations and that its boundary conditions are unique. This means that all approaches to Maxwell's equations express that the Helmholtz equation has the same and unique solution [26]. The method of separating variables (also known as the Fourier method) can be applied to the partial differential equation of (4). By letting $A_n(x, y) = A_{x,n}(x)\cdot A_{y,n}(y)$, we substitute into (4) to obtain

$$\frac{1}{A_{x,n}}\frac{d^2A_{x,n}}{dx^2} + \frac{1}{A_{y,n}}\frac{d^2A_{y,n}}{dy^2} + p_n^2 = 0 \quad (5)$$

Each of the terms with the second derivation in (5) must be equal to a constant because they must be independent of each other's denominator variables (x and y) and similarly for the third term. When defining that the first and second

terms are separation constants, $-k^2$ and γ_n^2, respectively, (5) is separated as follows:

$$\frac{d^2A_{x,n}}{dx^2} + k^2A_{x,n} = 0 \tag{6a}$$

$$\frac{d^2A_{y,n}}{dy^2} - \gamma_n^2A_{y,n} = 0 \tag{6b}$$

where k means the wave number along the x-axis and $k \in (0, \infty)$ and the wave number along the y-axis $\gamma_n = \sqrt{k^2 - p_n^2}$. The general solution to (6a) and (6b) is as follows:

$$A_{x,n} = G_s \cos k\,(x - x_s) + U_s \sin k\,(x - x_s) \tag{7a}$$

$$A_{y,n} = C_n e^{-\gamma_n y} + D_n e^{\gamma_n y} \tag{7b}$$

where G_s, U_s, C_n and D_n are unknown coefficients. $A(x - x_s, y) = A(-x + x_s, y)$ because of its symmetric structure, as shown in Fig. 1. Thus, $A_{x,n}$ in (7a) is an even function, resulting in only a cosine function ($U_s = 0$). The $e^{-\gamma_n y}$ and $e^{\gamma_n y}$ of $A_{y,n}$ in (7b) denote the forward and backward traveling waves along the y-axis, respectively, where the symbol e is the exponential constant. For all k, the solution for $A_n(x, y)$ can then be simplified to

$$A_n = \int_0^\infty \left[C_n e^{-\gamma_n y} + D_n e^{\gamma_n y}\right] G_s \cos k\,(x - x_s)dk \tag{8}$$

The magnetic field for the A_n with only z-component is obtained with the relations $B_{x,n} = \partial A_n(x, y)/\partial y$ and $B_{y,n} = -\partial A_n(x, y)/\partial x$.

$$B_{x,n} = \int_0^\infty \gamma_n \left[-C_n e^{-\gamma_n y} + D_n e^{\gamma_n y} \right] \cdot G_s \cos k\,(x - x_s)dk \tag{9a}$$

$$B_{y,n} = \int_0^\infty k \left[C_n e^{-\gamma_n y} + D_n e^{\gamma_n y} \right] \cdot G_s \sin k\,(x - x_s)dk \tag{9b}$$

where G_s is not absorbed into C_n and D_n to express explicitly the magnetic field intensity as a function of the amplitude and position of the current source. G_s depends on the initial condition of C_n, which is discussed in more detail in this section. The remaining set of unknown coefficients C_n and D_n can be obtained by enforcing boundary conditions for the magnetic field. According to the boundary condition, the tangential component $B_{x,n}$ and the normal component $B_{y,n}$ on an arbitrary interface of surfaces are described as follows:

$$\frac{B_{x,n-1}}{\mu_{n-1}} = \frac{B_{x,n}}{\mu_n} \tag{10a}$$

$$B_{y,n-1} = B_{y,n} \tag{10b}$$

where $B_{x,n-1}$ and $B_{y,n-1}$ are the magnetic fields at the interface for $y < T_n$, and $B_{x,n}$ and $B_{y,n}$ are the magnetic fields at the interface for $y > T_n$. For all x positions, the G_s of (8) are identical. Thus, only terms with subscript n on the right-hand side of (9a) and (9b) can be compared as follows:

$$\frac{\gamma_{n-1}}{\mu_{n-1}} \left[-C_{n-1}e^{-\gamma_{n-1}T_n} + D_{n-1}e^{\gamma_{n-1}T_n} \right] = \frac{\gamma_n}{\mu_n} \left[-C_n e^{-\gamma_n T_n} + D_n e^{\gamma_n T_n} \right] \tag{11a}$$

TABLE 1. Index of parameters.

Regions		Interfaces	
n	Parameters	n	Parameters
0	$\mu_0, \epsilon_0, \sigma_0, \gamma_0, p_0, C_0, D_0$		
1	$\mu_1, \epsilon_1, \sigma_1, \gamma_1, p_1, C_1, D_1$	1	W_1, T_1, M_1
2	$\mu_2, \epsilon_2, \sigma_2, \gamma_2, p_2, C_2, D_2$	2	W_2, T_2, M_2
...		...	
N	$\mu_N, \epsilon_N, \sigma_N, \gamma_N, p_N, C_N, D_N$	N	W_N, T_N, M_N

$$C_{n-1}e^{-\gamma_{n-1}T_n} + D_{n-1}e^{\gamma_{n-1}T_n} = C_n e^{-\gamma_n T_n} + D_n e^{\gamma_n T_n} \tag{11b}$$

The coefficients can be rewritten in matrix form as

$$\begin{bmatrix} C_{n-1} \\ D_{n-1} \end{bmatrix} = \begin{bmatrix} X_n\alpha_n & Y_n\beta_n \\ Y_n\beta_n^{-1} & X_n\alpha_n^{-1} \end{bmatrix} \tag{12}$$

with

$$X_n = (W_n + 1)/2$$
$$Y_n = (-W_n + 1)/2$$
$$\alpha_n = e^{\gamma_{n-1}T_n - \gamma_n T_n}$$
$$\beta_n = e^{\gamma_{n-1}T_n + \gamma_n T_n}$$

where $W_n = \mu_{n-1}\gamma_n/(\mu_n\gamma_{n-1})$. To avoid the confusion due to the index of interfaces and regions, Table 1 lists the index examples for the parameters used in this paper.

In the multilayer interface, the coefficient matrix $[M_n]$, which is a 2–by–2 matrix on the right-hand side of (12), combines the system's incident and outcome waves. Each element of $[M_n]$ is defined as $m_{11,n}$, $m_{12,n}$, $m_{21,n}$ and $m_{22,n}$. For example, $m_{12,n}$ represents the element in the first row and second column of M_n at Interface n. If there are no interfaces that create reflected waves in Region N, there is also no backward-traveling wave. Thus, M_N is the 2–by–1 matrix with $m_{11,N}$ and $m_{21,N}$. The target elements in (12) are C_{n-1} and D_{n-1} instead of C_n and D_n because it is difficult to obtain directly the backward-traveling wave related to D_0 in the current source region, unlike the forward-traveling wave related to C_0. The relationship between C_0, D_0, and C_N is expressed by $[M_n]$ multiplication for all interfaces $[M_{tot}]$.

$$\begin{bmatrix} C_0 \\ D_0 \end{bmatrix} = [M_1]\,[M_2]\ldots[M_N]\,C_N = [M_{tot}]\,C_N \tag{13}$$

where the elements of $[M_{tot}]$ are defined as $m_{11,tot}$ and $m_{21,tot}$, and C_N and D_0 can be expressed as $C_0/m_{11,tot}$ and $C_0 \cdot m_{21,tot}/m_{11,tot}$, respectively. In other words, if C_0 is set, C_N and D_0 are also determined by C_0. From (13), when viewed only from the viewpoint of the incident wave in the current source region, D_0 can be ignored and only the unknown $C_0 \cdot G_s$ remains. Here, $C_0 \cdot G_s$ can be obtained by Ampère's circuital law. For convenience, C_0 is set to 1. Even if C_0 is set to a

non-zero arbitrary value ($C_0 = 0$ means no incident wave), there is no problem because G_s changes accordingly. At $y = y_s$ and an arbitrary x-location in the current source region, the magnetic fields for the incident wave generated by the current source are $B_{x,0,inc} = 0$ and $B_{y,0,inc} = \mu_0 I_s/\{2\pi(x - x_s)\}$, where the subscript *inc* means an incident field. Comparing to (9b), $kC_0G_se^{-\gamma_0 y_n}$ must be equal to the result of the Fourier transform of the sine function for $B_{y,0,inc}$. Thus, when $C_0 = 1$, $G_s = \mu_0 I_s/(2\pi k)$. The magnetic field intensities, $H_{x,n}$ and $H_{y,n}$, are obtained by this G_s and $B = \mu H$.

$$H_{x,n} = \frac{I_s}{2\pi}\frac{\mu_0}{\mu_n}\int_0^\infty \frac{\gamma_n}{k}\left[-C_n e^{-\gamma_n y} + D_n e^{\gamma_n y}\right] \cdot e^{\gamma_0 y_s}\cos k\,(x - x_s)dk \tag{14a}$$

$$H_{y,n} = \frac{I_s}{2\pi}\frac{\mu_0}{\mu_n}\int_0^\infty \left[C_n e^{-\gamma_n y} + D_n e^{\gamma_n y}\right] \cdot e^{\gamma_0 y_s}\sin k\,(x - x_s)dk \tag{14b}$$

B. SHIELDING METRICS

The shielding effectiveness for material properties, SE_M, is a significant parameter that indicates the degree to which shielding materials attenuate the strength of incident waves at an interface. SE_M is defined as the ratio of the magnitude of the incident magnetic field intensity at Interface 1, $H_{i,0}$, to the magnitude of the transmitted magnetic field intensity at Interface N, $H_{t,N}$. That is, $SE_M = |H_{t,N}|/|H_{i,0}|$. As shown in (14a), the maximum magnitude of $H_{i,1}$ is located at $x = x_s$ and $y = 0$, which is the shortest distance between the current source and Interface 1. As with $H_{i,0}$, the set of positions for $H_{t,N}$ is $x = x_s$ and $y = T_N$. From (14), both $H_{i,1}$ and $H_{t,N}$ corresponding to each position have only the x-component ($H_{y,n} = 0$). In particular, $|H_{i,0}| = |I_s/(2\pi y_s)|$. Thus, the dB-scale of SE_M, $SE_{M,dB}$, can be expressed as

$$SE_{M,dB} = 20\log\left|\frac{\mu_0}{\mu_N}y_s\int_0^\infty \frac{\gamma_N}{k}\left[C_N e^{-\gamma_N T_N}\right]e^{\gamma_0 y_s}dk\right| \tag{15}$$

The geometrical shielding effectiveness of the shielding materials, SE_G, is defined differently from SE_M. For instance, if SE_G is defined as being equal to SE_M, T_N in (15) also increases as the thickness of the shielding material in Region 1 increases. This means that SE_G includes not only the effect of the geometrical properties of shielding materials but also the effect of monotonically increasing the measurement position. Thus, SE_G should be defined at an arbitrary fixed $y_q > T_N$.

$$SE_{G,dB} = 20\log\left|\frac{\mu_0}{\mu_N}y_s\int_0^\infty \frac{\gamma_N}{k}\left[C_N e^{-\gamma_N y_q}\right]e^{\gamma_0 y_s}dk\right| \tag{16}$$

Although the shielding effectiveness is related to the magnetic field intensity in the shielding region, a reflection coefficient, Γ_M, which affects the magnetic field intensity in the current source region, is also the significant parameter. Γ_M at $x = x_s$ and $y = 0$ corresponding to Interface 1, is defined as the ratio of $H_{i,0}$ to the magnitude of the reflected magnetic field intensity, $H_{r,0}$. That is, $\Gamma_M = H_{r,0}/H_{i,0}$. As $H_{r,0}$ has only the x-component and is the reflection wave, it can be expressed as the term ignoring C_0 from (14a). Thus, Γ_M can be derived as follows:

$$\Gamma_M = y_s\int_0^\infty \frac{\gamma_0}{k}\left[D_0\right]e^{\gamma_0 y_s}dk \tag{17}$$

The sign of the real part for Γ_M indicates whether interference is constructive or destructive. If "+" is obtained, the magnetic field intensity in the current source region increases along the vertical line of Interface 1 passing through $x = x_s$ and $y = 0$.

TABLE 2. Electrical properties of shielding materials.

	MM.1	MM.2	air.	CM.1	CM.2
μ_r	10^3	10^4	1	1	1
ϵ_r	1	1	1	1	1
σ	0	0	0	3.8×10^6	3.8×10^7

TABLE 3. Configuration of shielding materials.

case	Region1	Region2	Region3
1	MM.1	air.	CM.1
2	CM.1	"	MM.1
3	MM.2	"	CM.1
4	CM.1	"	MM.2

III. PARAMETRIC ANALYSIS FOR SHIELDING MATERIALS

A parametric analysis was performed to study the influence of the geometrical and electrical parameters of the shielding material. Table 2 lists the electrical properties of the materials used for the parametric analysis. Here, the relative permeability and permittivity are expressed as μ_r and ϵ_r, respectively, and the magnetic material, air-gap, and conductive material are expressed in abbreviated form as MM., ari., and CM., respectively. The analysis conditions for the electrical property combinations of these materials are listed in Table 3 where the thicknesses of Regions, 1, 2, and 3 are 0.01, 0.001, and 0.01 [m], respectively. Commonly, the current source in all cases is located at $x_s = 0$ and $y_s = -1$ [m], and its current is $I_s = 100$ [A]; the current source and shielding region have the same electrical properties as vacuum.

A. ARRANGEMENT OF SHIELDING MATERIALS

In Cases 1 and 2, the contours of the dB-scale ($20\log 10|H|$) for the maximum magnetic field intensity at an arbitrary location are plotted in Fig. 2. When the positions of MM.1 and CM.1 are exchanged, the distribution of the magnetic field intensity in the shielding region hardly changes, whereas that in the current source region changes. Fig. 3 shows a plot of magnetic field intensity along the vertical line passing through $x = 0$. It is clear from Fig. 3 that a magnetic material maintains a low magnetic field intensity over the entire region occupied by this material, whereas a conductive material causes the magnetic field intensity to drop drastically.

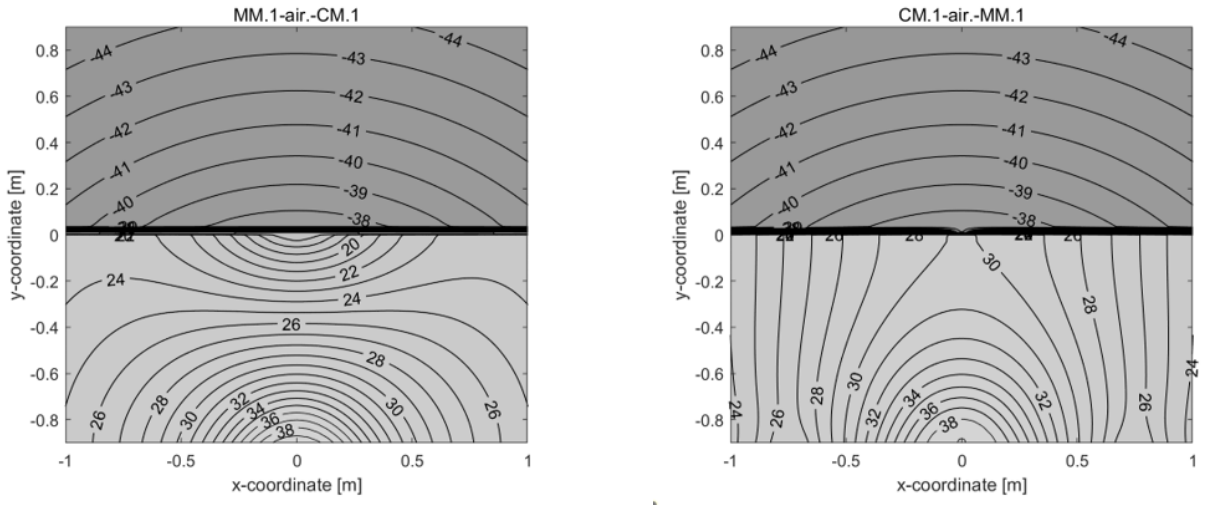

FIGURE 2. Contours of $20\log 10|\boldsymbol{H}|$ for two cases: (a) MM.1–air.–CM.1 and (b) CM.1–air.–MM.1. Comparing the two cases, the magnetic field intensity in the shielding region is identical, but that in the current source region is not.

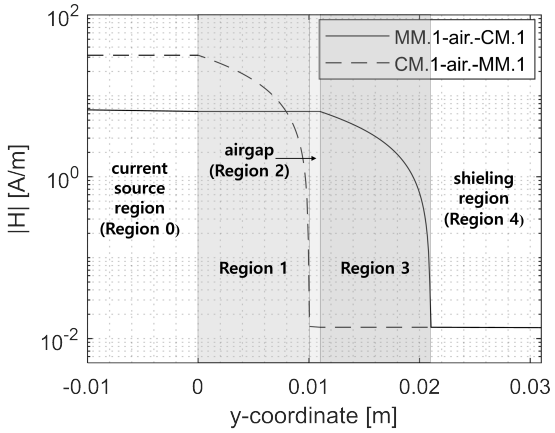

FIGURE 3. Maximum magnetic field intensity along the vertical line (-0.01 [m] $\le y \le 0.03$ [m], $x = 0$) for the two cases.

From the same magnetic field intensity in the shielding region, it can be inferred that each shielding material has its own shielding efficiency, regardless of the influence of the other adjacent materials. The plots of the magnetic field intensity along the horizontal line passing through $y_q = -0.01$ [m] and $y_q = 0.031$ [m] are shown in Fig. 4. Both cases have the same $SE_{M,dB} = -60.435$ [dB]. Thus, the exchange in position of the conductive and magnetic materials is not a crucial factor in reducing the magnetic field intensity in the shielding region. However, the impact differs in the current source region. In the case of MM.1–air.–CM.1, $\Gamma_{M,re}$, which is the real part of Γ_M, is –0.952, which means that the magnetic field intensity can be reduced by destructive interference, whereas conversely, $\Gamma_{M,re} = 0.842$, the magnetic field intensity increases due to constructive interference. The impedance difference between the two regions abutting Interface 1 determines the sign of $\Gamma_{M,re}$. Although the magnetic field region covered in this study is assumed to be near-field due to the 50 or 60 [Hz] operating frequency, the characteristic impedance and reflection coefficient for far-field can be qualitatively applied even for the near-field. The characteristic impedance increases as the permeability increases, whereas it decreases as the conductivity increases. The characteristic impedance of Region 1 with high permeability is bigger than that of the current source region. Thus, the reflection coefficient has the "+" sign. Because the reflection coefficient for the far-field is defined based on the electric field, it has the opposite sign when defined based on magnetic field intensity, as in Γ_M of this study. Changes in $\Gamma_{M,re}$ and SE_M for relative permeability and conductivity will be discussed in more detail in subsections B and C of this section. The parametric analysis is performed with only one parameter modified at a time and the other dimensions maintained at the previously defined reference values.

B. PERMEABILITY OF SHIELDING MATERIALS

As shown in Fig. 5, the magnetic field intensity in the shielding region decreased as the relative permeability decreased, regardless of the arrangement of the shielding material. The high relative permeability of the shielding material concentrates more magnetic fields per unit cross-sectional area than materials with relatively low relative permeability. The magnetic field intensity in the shielding region can decrease because of this impact. A comparison of the result of Figs. 5a and 5c shows that the magnetic field intensity in the current source region is more affected by the change in the relative permeability of the immediately adjacent region. As shown in Fig. 5a, for the MM.2–air.–CM.1 case, the magnetic field intensity is reduced because the relative permeability of MM.2 is 10 times higher than that of MM.1.

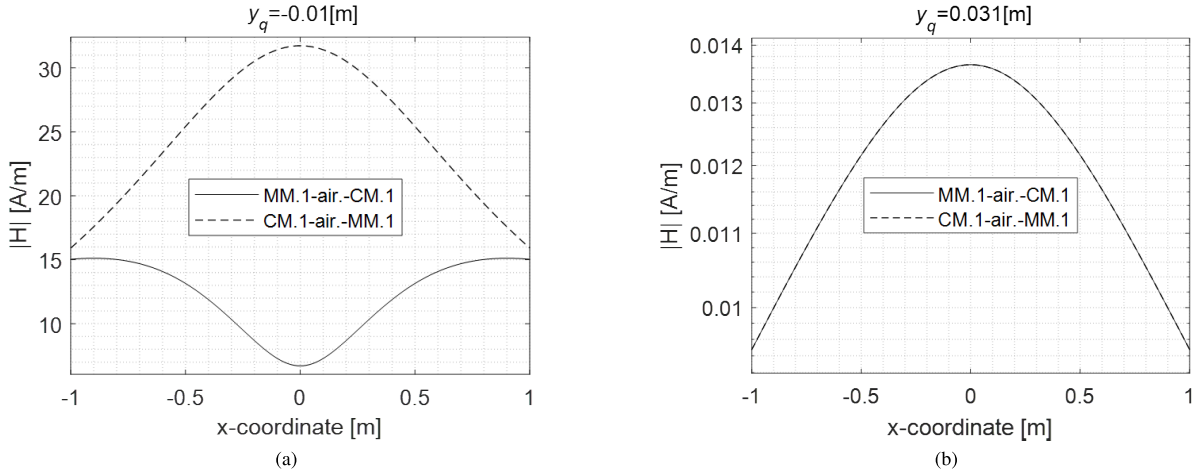

FIGURE 4. Maximum magnetic field intensity along the horizontal lines of (a) the current source region (-1 [m] $\leq x \leq 1$ [m], $y_q = -0.01$ [m]) and (b) shielding region (-1 [m] $\leq x \leq 1$ [m], $y_q = 0.031$ [m]) for the two cases.

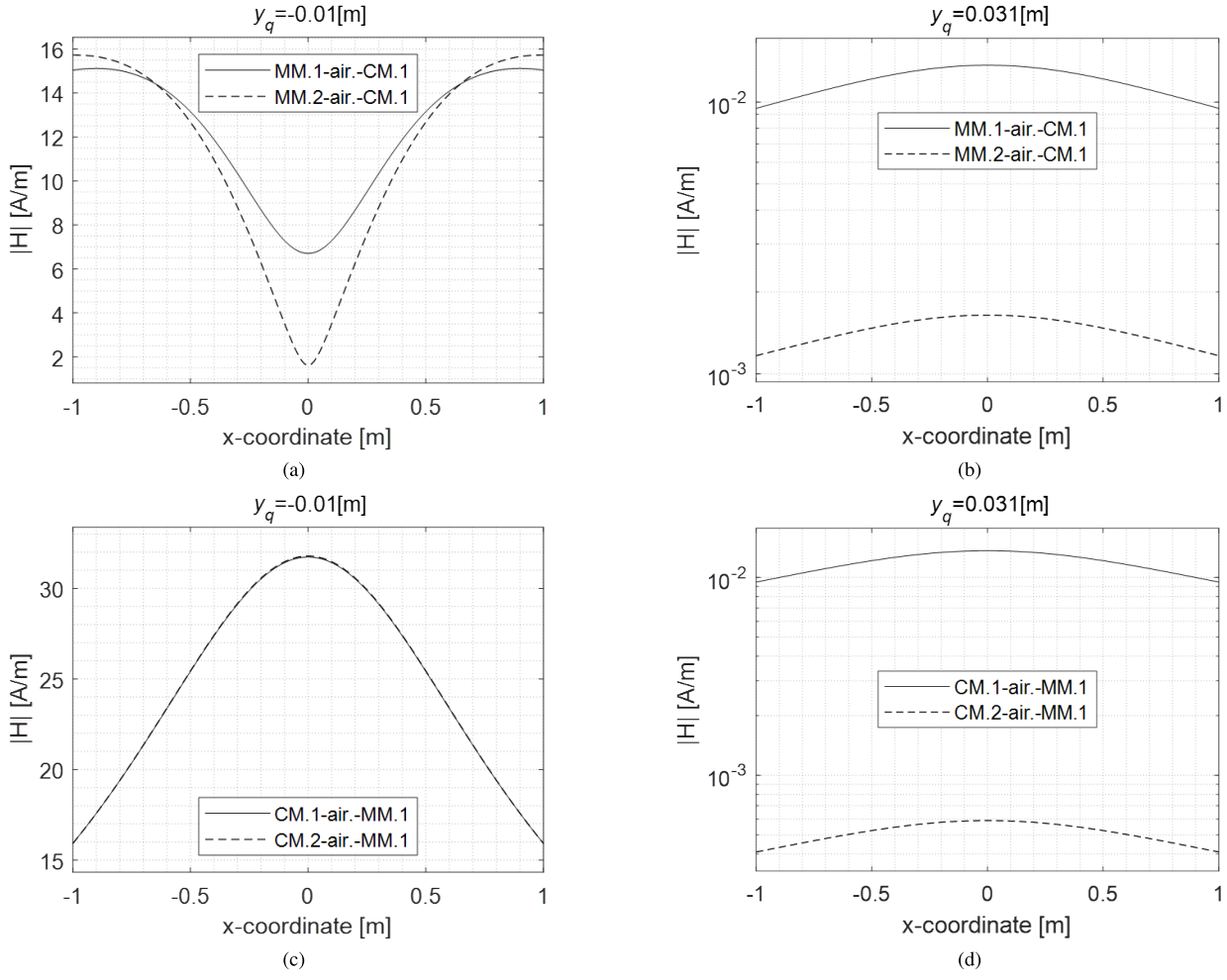

FIGURE 5. Maximum magnetic field density for a change in magnetic material (permeability). (a) and (c) are obtained by the current source region (-1 [m] $\leq x \leq 1$ [m], $y_q = -0.01$ [m]), and (b) and (d) are obtained by the current source region (-1 [m] $\leq x \leq 1$ [m], $y_q = 0.031$ [m]).

However, as shown in Fig. 5c, even if the relative permeability of non-adjacent materials in the current region changes, the magnetic field intensities in the current source region are nearly the same. Fig. 6 shows more detailed analysis for $\Gamma_{M,re}$ and $SE_{M,dB}$ performed by increasing the relative permeability from 1 to 10^8 with fixed conductivity. As the

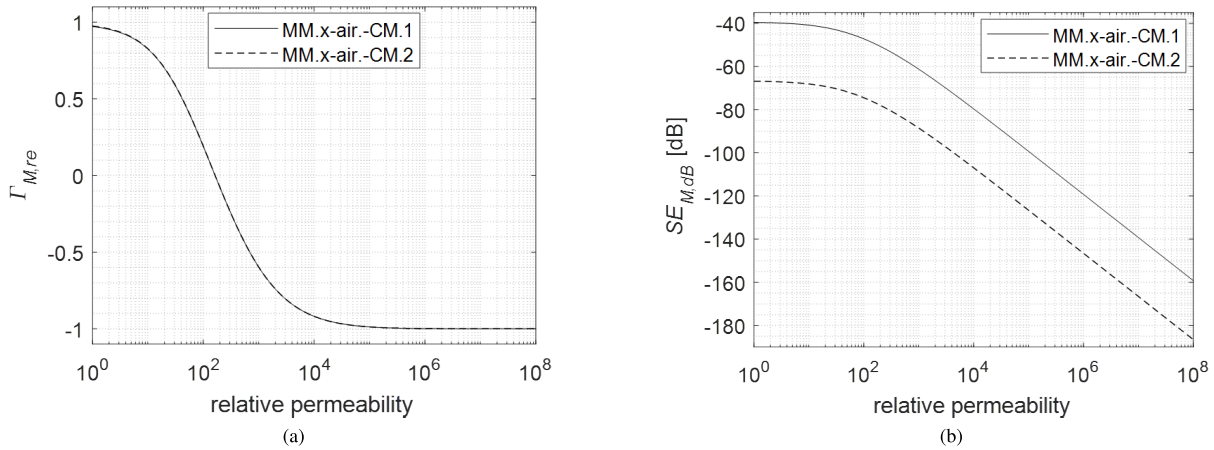

FIGURE 6. (a) $\Gamma_{M,re}$ and (b) $SE_{M,dB}$ for a change in relative permeability.

relative permeability increases, $\Gamma_{M,re}$ becomes closer to -1, where the "$-$" sign means the opposite phase for an incident magnetic field intensity. If the relative permeability has a value of 160 or less, $\Gamma_{M,re}$ has the "$+$" sign owing to the permittivity and conductivity of this material. Changes in the conductivity of materials non-adjacent in the current source region do not significantly affect Γ_M, whereas they make the difference in $SE_{M,dB}$ around 26 [dB] over the all ranges of relative permeability.

C. CONDUCTIVITY OF SHIELDING MATERIALS

An increase in the conductivity of the shielding material can reduce the magnetic field intensity in the shielding region, as shown in Fig. 7. Some of the magnetic field energy transmitted through the shielding material is absorbed owing to the loss characteristics of this material, and the increase in conductivity increases the degree of energy absorption. Compared with Fig. 5a for permeability, the change in the magnetic field intensity in the current source region for conductivity is not noticeable, as shown in Fig. 7a. The $\Gamma_{M,re}$ values for conductivity are illustrated in Fig. 8a. The difference between $\Gamma_{M,re}$ for the conductivity of CM.1 and CM.2 is merely 0.01, as can be observed in Fig. 7c. As the conductivity increases, the sign of $\Gamma_{M,re}$ changes from "$-$" to "$+$" based on $\sigma = 1.32 \times 10^5$ [S/m]. When $\sigma > 1.32 \times 10^5$ [S/m], the magnetic field intensity in the current source region increases due to constructive interference, and the permeability of the material in Region 3 has not effect on $\Gamma_{M,re}$. However, when $\sigma < 1.32 \times 10^5$ [S/m], the magnetic field intensity in the current source region decreases due to destructive interference, and as the permeability of the material in Region 3 increases, $\Gamma_{M,re}$ converges to -1. Fig. 8b shows that the shielding effect occurs at a conductivity of more than a specific value. The specific value depends on the permeability of the material which is in Region 3; however, under a condition given in Fig. 8, the shielding effect is insignificant at $\sigma < 10^4$ [S/m].

D. THICKNESSES OF SHIELDING MATERIALS AND AN AIR-GAP

The $\Gamma_{M,re}$ and $SE_{G,dB}$ values with a change in the thickness of each shielding material are shown in Fig. 9, where the y-location, y_q, to obtain $SE_{G,dB}$ is 0.031 [m]. As the thickness increases, more magnetic field energy is stored in the shield or the conduction loss increases more. The impact reduces the magnetic field intensity in the shielding region regardless of the arrangement of the shielding material, as shown in Fig. 9. As mentioned above, $\Gamma_{M,re}$ is the parameter that affects the magnetic field intensity in the current source region, and $\Gamma_{M,re}$ changes according to the thickness of the material adjacent in this region. Fig. 9a shows that the sign of $\Gamma_{M,re}$ varies based on MM.1 thickness at 1.65×10^{-3} [m], and this means that the magnetic field intensity in the current source region can reduce more beyond a certain thickness. As shown in Fig. 9c, the increasing thickness of CM.1 adjacent in the current source region rather increases the magnetic field intensity in this region. In addition, unlike MM.1, $\Gamma_{M,re}$ of CM.1 has the "$+$" sign on all thickness range. Fig. 10 shows the impact for air-gap thickness. $\Gamma_{M,re}$ has a constant value regardless of the air-gap thickness. $SE_{G,dB}$ changes with increasing air-gap thickness, but the impact of this thickness is insignificant as the difference between the maximum and minimum of $SE_{G,dB}$ in Fig. 10b is merely 0.09 [dB].

IV. SHIELDING PIPE

Prior to using shielding materials to reduce the magnetic field intensity in the shielding region, the current source was wrapped with a shielding pipe [27], [28]. Under this condition, the incident magnetic field intensity at Interface 1 changes. Fig. 11 shows the basic configuration of the current source and its shielding pipe, which mitigate the magnetic field intensity incident on Interface 1. Owing to the uniform and infinitely long structure in the z-direction, the magnetic vector potential of the cylindrical coordinate, $A_{n,wp}$ has only the z-component, and is expressed only as a function of the radial distance, r, from the center of the

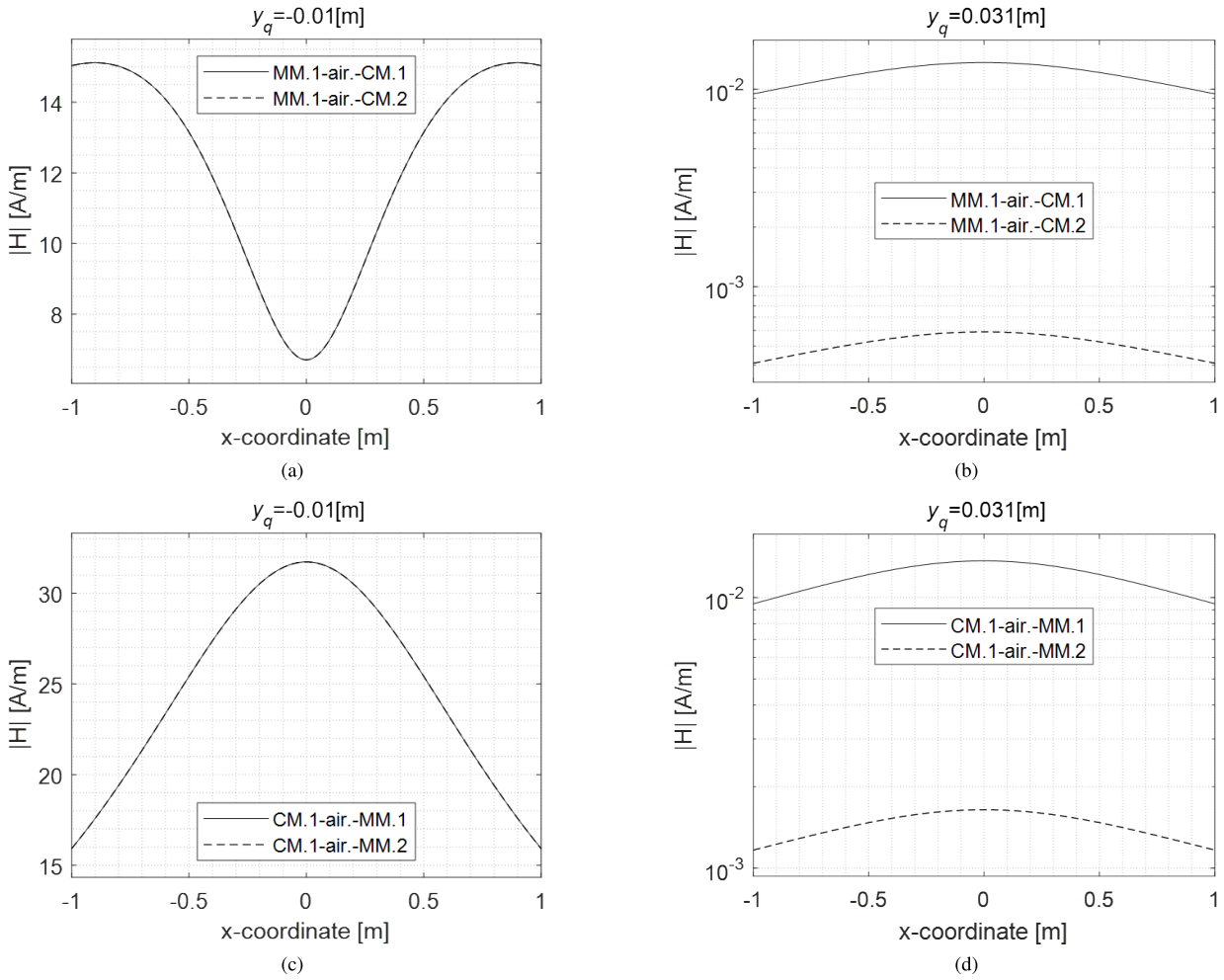

FIGURE 7. Maximum magnetic field density for a change in conductive material (conductivity). (a) and (c) are obtained by the current source region. (a) and (c) are obtained by the current source region (-1 [m] $\leq x \leq 1$ [m], $y_q = -0.01$ [m]), and (b) and (d) are obtained by the current source region (-1 [m] $\leq x \leq 1$ [m], $y_q = 0.031$ [m]).

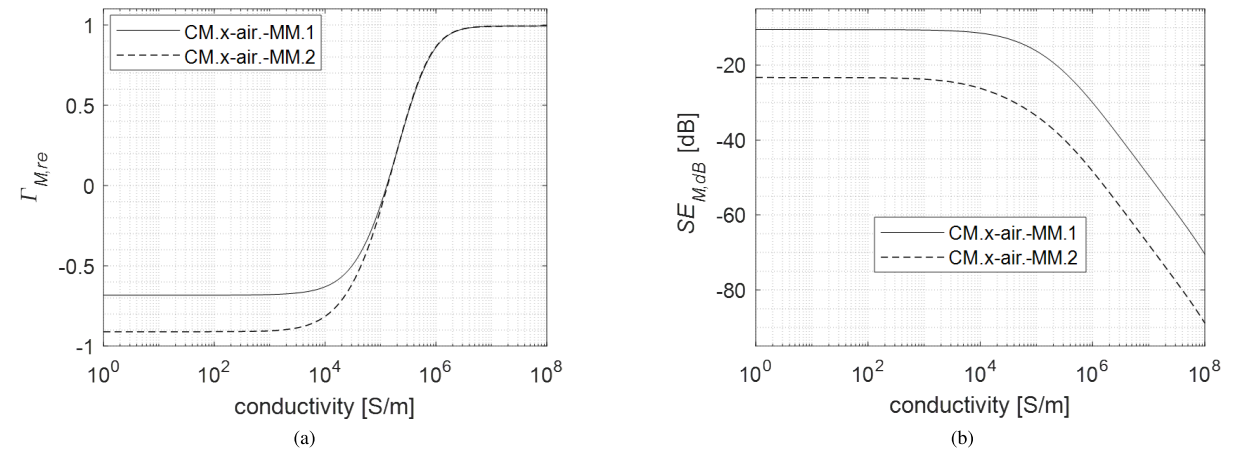

FIGURE 8. (a) $\Gamma_{M,re}$ and (b) $SE_{M,dB}$ for a change in conductivity.

current source.

$$\left(\frac{d^2}{dx^2} + \frac{1}{r}\frac{d^2}{dr^2} + p_n^2\right) A_{n,wp}(r) = 0 \tag{18}$$

where subscript n indicates the shielding pipe region (Region s) and the current source region (Region 0), denoted by s and 0, respectively. For each region, the solution of (18)

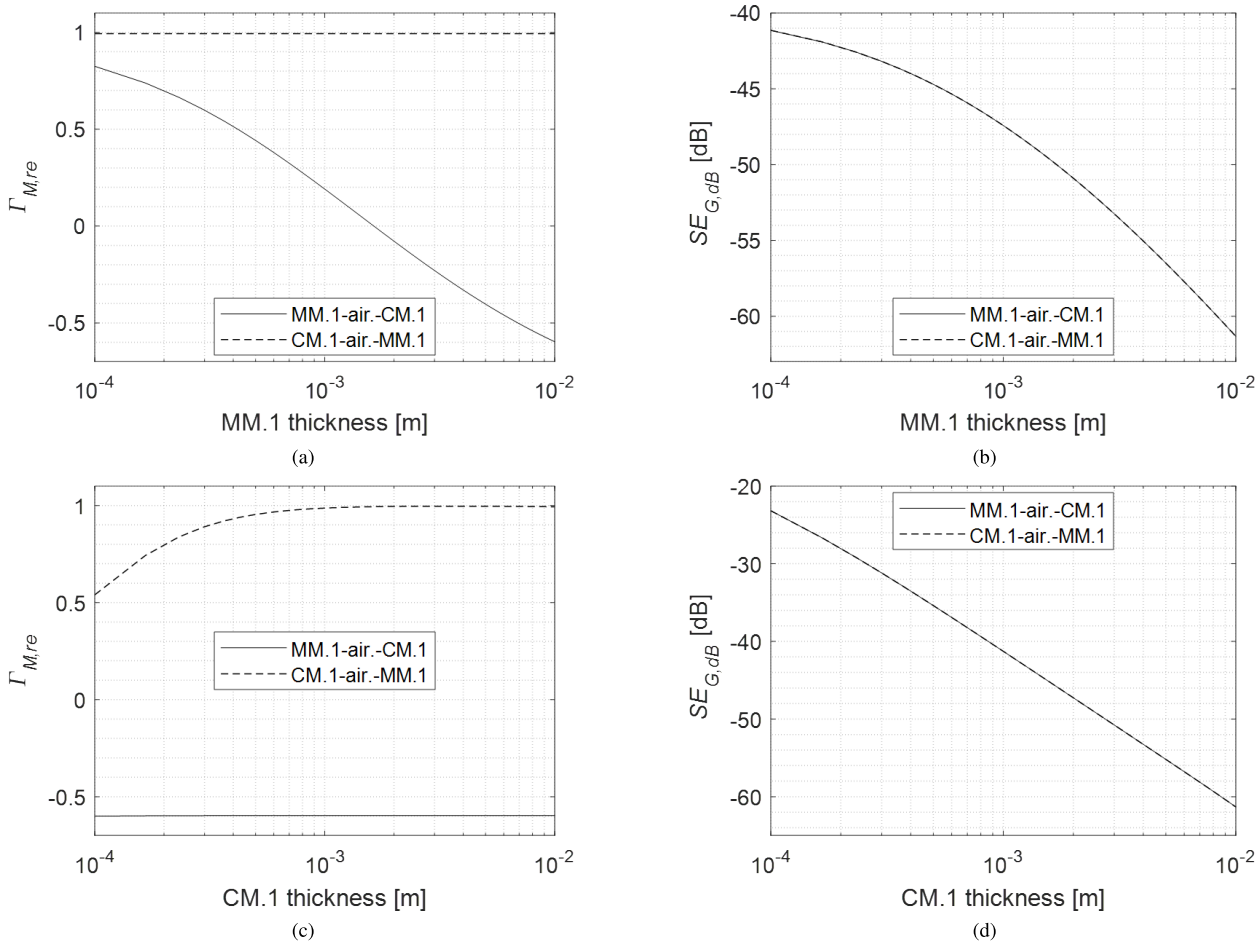

FIGURE 9. $\Gamma_{M,re}$ and $SE_{M,dB}$ for a change in thickness of the shielding material. (a) and (b) are obtained by increasing MM1. thickness, and (c) and (d) are obtained by increasing CM.1. thickness.

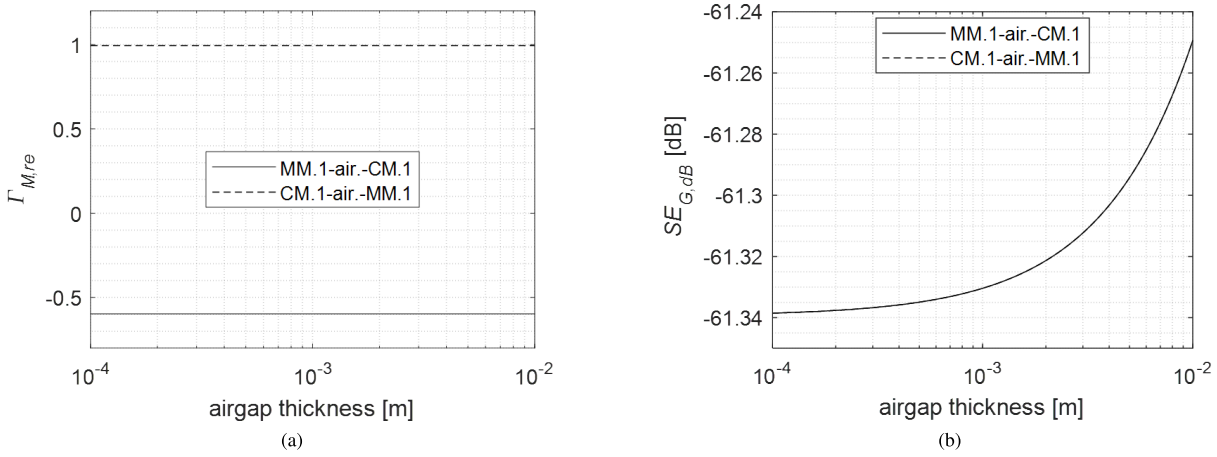

FIGURE 10. (a) $\Gamma_{M,re}$ and (b) $SE_{G,dB}$ for a change in an airgap thickness.

can be obtained as follows:

$$A_{s,wp}(r) = c_0 \mathrm{H}_0^{(1)}(p_s r) + c_1 \mathrm{H}_0^{(2)}(p_s r) \quad (19a)$$

$$A_{s,0}(r) = c_2 \mathrm{H}_0^{(1)}(p_0 r) \quad (19b)$$

where $\mathrm{H}_0^{(1)}$ and $\mathrm{H}_0^{(2)}$ are 0th-order Hankel functions of the first and second kinds, respectively, and c_0, c_1, and c_2 are unknown coefficients. From $B_\phi = \partial A(r)/\partial r$ and $H = B/\mu$, the magnetic field intensity can be

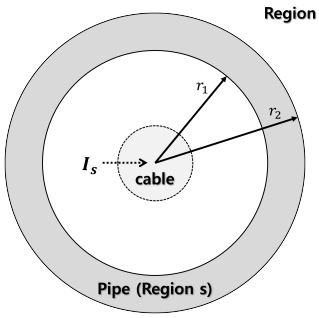

FIGURE 11. Basic configuration of shielding pipe for two cases.

expressed as

$$H_{\phi,s,wp}(r) = c_0 \frac{p_s}{\mu_s} \mathrm{H}_0^{(1)}(p_s r) + c_1 \frac{p_s}{\mu_s} \mathrm{H}_0^{(2)}(p_s r) \quad (20a)$$

$$H_{\phi,0,wp}(r) = c_2 \frac{p_0}{\mu_0} \mathrm{H}_0^{(1)}(p_0 r) \quad (20b)$$

where $\mathrm{H}_1^{(1)}$ and $\mathrm{H}_0^{(2)}$ are 1st-order Hankel functions of the first and second kinds, respectively. The three unknown coefficients can be determined using the three boundary conditions of magnetic field intensity and magnetic vector potential. That is, using the coefficients obtained by $I_s/(2\pi r_1) = H_{\phi,s,wp}(r_1)$, $H_{\phi,s,wp}(r_2) = H_{\phi,0,wp}(r_2)$ and $A_{s,wp}(r_2) = A_{0,wp}(r_2)$, the forward magnetic field intensity, $H_{\phi,0,wp}(r)$, in the current source region can be expressed as

$$H_{\phi,0,wp}(r) = \frac{I_s}{2\pi r_1} \frac{\mathrm{H}_1^{(2)}(p_s r_2) - \kappa \cdot \mathrm{H}_1^{(1)}(p_s r_2)}{\mathrm{H}_1^{(2)}(p_s r_1) - \kappa \cdot \mathrm{H}_1^{(1)}(p_s r_1)} \frac{\mathrm{H}_1^{(2)}(p_0 r)}{\mathrm{H}_1^{(1)}(p_0 r_2)} \quad (21)$$

with

$$\kappa = \frac{\mu_0 p_s \mathrm{H}_1^{(2)}(p_s r_2)\,\mathrm{H}_0^{(1)}(p_0 r_2) - \mu_s p_0 \mathrm{H}_0^{(2)}(p_s r_2)\,\mathrm{H}_1^{(1)}(p_0 r_2)}{\mu_0 p_s \mathrm{H}_1^{(1)}(p_s r_2)\,\mathrm{H}_0^{(1)}(p_0 r_2) - \mu_s p_0 \mathrm{H}_0^{(1)}(p_s r_2)\,\mathrm{H}_1^{(1)}(p_0 r_2)}$$

V. APPLICATION TO SHIELDING CONFIGURATION

An example of shielding configuration based on the results of the previous sections is illustrated in this section. As mentioned above, the arrangement of the shielding material does not affect the magnetic field intensity of the shielding region, but it has the opposite effect in the current source region. Placing a conductive material in Region 1 allows the magnetic material in Region 3 to be free from magnetic saturation because of the high conductivity loss of the conductive material. However, in the current source region, the magnetic field intensity increases because of constructive interference. Thus, to reduce the magnetic field intensity in the current source region, the magnetic material should first be placed in Region 1, and installed at an appropriate distance from the current source to avoid the start of magnetic saturation.

The use of a composite material having a relatively high conductivity and outstanding magnetic material property ($\Gamma_{M,re} < 0$) can mitigate the magnetic field intensity in the region where the field is incident, with the advantage of a high attenuation for the transmitted magnetic field.

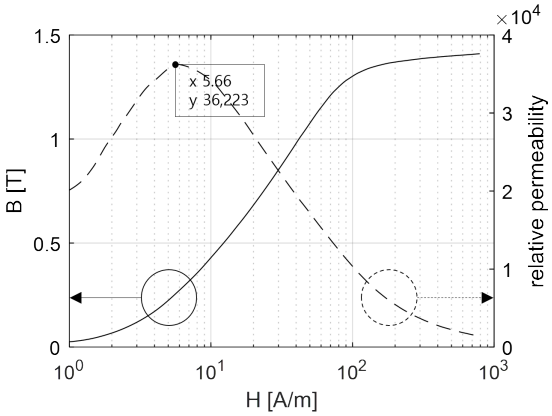

FIGURE 12. *B–H* curve (solid line) and relative permeability (dashed line) for the two cases.

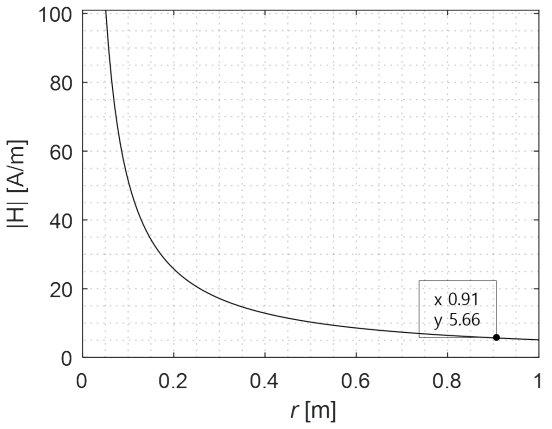

FIGURE 13. Maximum magnetic field intensity at distance, *r*, from the center of the current source.

A magnetic alloy with conductivity of 7.25×10^5 [S/m], is employed in Region 1 to reduce the magnetic field intensity in the current source region. Its nonlinear characteristics are shown in Fig. 12, including its relative permeability and the incident magnetic field intensity at which magnetic saturation begins. The maximum relative permeability is 36,233 at $|H| = 5.66$ [A/m], indicating maximum shielding efficiency. Region 2 is occupied by aluminum whose the electrical property is the same as that of CM.1 in Table 2. Here, the air-gap is ignored because its thickness has little effect on the change in the magnetic field intensity as shown in Fig. 10. The thicknesses of Regions 1 and 2 are equal to 0.005 [m]. The shielding pipe discussed in this section is made of copper ($\sigma = 3.8 \times 10^7$ [S/m]), and its geometrical parameters are $r_1 = 0.05$ [m] and $r_2 = 0.001$ [m]. The magnetic field intensity generated by the cable decreases drastically as it passes through the shield pipe, and then it is incident on Interface 1. When $I_s = 750$ [A], the incident magnetic field intensity calculated in accordance with distance r from the cable center using (21) is shown in Fig. 13. Here, $r = 0.91$ [m] corresponding to $|H| = 5.66$ [A/m]. To simplify calculations, the current source that generates this magnetic field is assumed to be an equivalent point source. In this shielding configuration,

$\Gamma_{M,re}$ and $SE_{M,dB}$ obtained by (15) and (17) are -0.66 and -157 [dB], respectively.

VI. CONCLUSION

In this paper, the principles of shielding materials are discussed, and a simple guideline for the shielding configuration is presented using these principles. The discussion is based on mathematical expressions for the shielding effectiveness and reflection coefficient. Various parametric analyses have been conducted to determine the best shield configuration based the geometrical and electrical parameters of the shielding materials. The results show that these parameters have significant effects not only on the shielding region but also on the current source region. The graphs with comparative data presented in this paper intuitively show the effects of these parameters. In addition, the change in magnetic field intensity due to the shielding pipe wrapping of the current source was calculated. Then, the permeability corresponding to its magnetic field intensity from a nonlinear *B–H* curve was obtained, resulting in the determination of the optimal distance between the current source and the shielding materials. The shielding configuration can be summarized as follows: 1) The arrangement order of the conductive and magnetic materials does not affect the changes in the magnetic field intensity of the shielding region. 2) The magnetic field intensity reflected on the magnetic material with a certain thickness or greater has the opposite phase of the incident field. 3) The magnetic field intensity reflected on the conductive material has the same phase as that of the incident field. 4) To reduce the magnetic field intensity in the current source region, the magnetic material should be placed first, and the conductive material should be placed next. 5) The gap between the magnetic and conductive materials does not significantly change the magnetic field intensity in either the current source and shielding regions. 6) The magnetic material should be kept at an appropriate distance from the current source to prevent magnetic saturation and maximize the shielding effectiveness.

REFERENCES

[1] J. Bravo-Rodríguez, J. del-Pino-López, and P. Cruz-Romero, "A survey on optimization techniques applied to magnetic field mitigation in power systems," *Energies*, vol. 12, no. 7, p. 1332, Apr. 2019, doi: 10.3390/EN12071332.

[2] J. Grellier, P. Ravazzani, and E. Cardis, "Potential health impacts of residential exposures to extremely low frequency magnetic fields in Europe," *Environ. Int.*, vol. 62, pp. 55–63, Jan. 2014.

[3] A. Huss, S. Peters, and R. Vermeulen, "Occupational exposure to extremely low-frequency magnetic fields and the risk of ALS: A systematic review and meta-analysis: Exposure to magnetic fields and ALS," *Bioelectromagnetics*, vol. 39, no. 2, pp. 156–163, Feb. 2018.

[4] H. Zhou, G. Chen, C. Chen, Y. Yu, and Z. Xu, "Association between extremely low-frequency electromagnetic fields occupations and amyotrophic lateral sclerosis: A meta-analysis," *PLoS ONE*, vol. 7, no. 11, Nov. 2012, Art. no. e48354.

[5] H. C. Lee, M.-N. Hong, S. H. Jung, B. C. Kim, Y. J. Suh, Y.-G. Ko, Y.-S. Lee, B.-Y. Lee, Y.-G. Cho, S.-H. Myung, and J.-S. Lee, "Effect of extremely low frequency magnetic fields on cell proliferation and gene expression," *Bioelectromagnetics*, vol. 36, no. 7, pp. 506–516, Oct. 2015.

[6] W. Van Loock, "Elementary effects in humans exposed to electromagnetic fields and radiation," in *Proc. 5th Asia–Pacific Conf. Environ. Electromagn.*, Xian, China, Sep. 2009, pp. 221–224.

[7] G. A. Florea, A. Dinca, and S. I. A. Gal, "An original approach to the biological impact of the low frequency electromagnetic fields and proofed means of mitigation," in *Proc. IEEE Bucharest PowerTech*, Bucharest, Romania, Jul. 2009, pp. 1–8.

[8] J. Lin, R. Saunders, K. Schulmeister, P. Söderberg, B. E. Stuck, A. Swerdlow, M. Taki, B. Veyret, G. Ziegelberger, M. H. Repacholi, R. Matthes, A. Ahlbom, K. Jokela, and C. Roy, "ICNIRP guidelines for limiting exposure to time-varying electric, magnetic and electromagnetic fields (1 Hz to 100 kHz)," *Health Phys.*, vol. 99, no. 6, pp. 818–836, Dec. 2010. [Online]. Available: https://hal.univ-grenoble-alpes.fr/IMS-BORDEAUX-FUSION/hal-01019994 and https://www.icnirp.org/cms/upload/publications/ICNIRPLFgdl.pdf

[9] Y.-L. Song, M. K. Reddy, H.-Y. Wen, and L.-M. Chang, "Mitigation of electro magnetic interference by using C-shaped composite cylindrical device," *Appl. Sci.*, vol. 12, no. 2, p. 882, Jan. 2022.

[10] M. Mitolo, F. Freschi, M. Pastorelli, and M. Tartaglia, "Ecodesign of low-voltage systems and exposure to ELF magnetic fields," *IEEE Trans. Ind. Appl.*, vol. 47, no. 2, pp. 984–988, Mar. 2011.

[11] *Mitigation Techniques of Power-Frequency Magnetic Fields Originated From Electric Power Systems*. CIGRÉ Tech. Brochure, CIGRÉ, Paris, France, Aug. 2009.

[12] M. Reta-Hernández and G. G. Karady, "Attenuation of low frequency magnetic fields using active shielding," *Electr. Power Syst. Res.*, vol. 45, no. 1, pp. 57–63, Apr. 1998.

[13] Y. Du and N. Xia, "Principles of power-frequency magnetic shielding with finite-width plates," *Int. Trans. Electr. Energy Syst.*, vol. 24, no. 8, pp. 1168–1184, Aug. 2014.

[14] A. Canova, J. C. del-Pino-Lopez, L. Giaccone, and M. Manca, "Active shielding system for ELF magnetic fields," *IEEE Trans. Magn.*, vol. 51, no. 3, pp. 1–4, Mar. 2015.

[15] J. C. del Pino Lopez and P. C. Romero, "The effectiveness of compensated passive loops for mitigating underground power cable magnetic fields," *IEEE Trans. Power Del.*, vol. 26, no. 2, pp. 674–683, Apr. 2011.

[16] U. Jonsson, A. Larsson, and J.-O. Sjodin, "Optimized reduction of the magnetic field near Swedish 400 KV lines by advanced control of shield wire currents. Test results and economic evaluation," *IEEE Trans. Power Del.*, vol. 9, no. 2, pp. 961–969, Apr. 1994.

[17] Y. Du, T. C. Cheng, and A. S. Farag, "Principles of power-frequency magnetic field shielding with flat sheets in a source of long conductors," *IEEE Trans. Electromagn. Compat.*, vol. 38, no. 3, pp. 450–459, Aug. 1996.

[18] R. G. Olsen, M. Istenic, and P. Zunko, "On simple methods for calculating ELF shielding of infinite planar shields," *IEEE Trans. Electromagn. Compat.*, vol. 45, no. 3, pp. 538–547, Aug. 2003.

[19] M. Istenic and R. G. Olsen, "A simple hybrid method for ELF shielding by imperfect finite planar shields," *IEEE Trans. Electromagn. Compat.*, vol. 46, no. 2, pp. 199–207, May 2004.

[20] A. Canova, A. Manzin, and M. Tartaglia, "Evaluation of different analytical and semi-analytical methods for the design of ELF magnetic field shields," *IEEE Trans. Ind. Appl.*, vol. 38, no. 3, pp. 788–796, May 2002.

[21] S.-B. Kim, J.-Y. Soh, K.-Y. Shin, J.-H. Jeong, and S.-H. Myung, "Magnetic shielding performance of thin metal sheets near power cables," *IEEE Trans. Magn.*, vol. 46, no. 2, pp. 682–685, Feb. 2010.

[22] J. C. D. Pino-Lopez and P. Cruz-Romero, "Magnetic field shielding of underground cable duct banks," *Prog. Electromagn. Res.*, vol. 138, pp. 1–19, 2013.

[23] J. C. del-Pino-López, P. Cruz-Romero, L. Serrano-Iribarnegaray, and J. Martínez-Román, "Magnetic field shielding optimization in underground power cable duct banks," *Electr. Power Syst. Res.*, vol. 114, pp. 21–27, Sep. 2014.

[24] T. Morisue, "Magnetic vector potential and electric scalar potential in three-dimensional eddy current problem," *IEEE Trans. Magn.*, vol. MAG-18, no. 2, pp. 531–535, Mar. 1982.

[25] D. J. Griffiths, *Introduction to Electrodynamics*. Upper Saddle River, NJ, USA: Prentice-Hall, 2013.

[26] A. T. de Hoop, "A time-domain uniqueness theorem for electromagnetic wavefield modeling in dispersive, anisotropic media," *Radio Sci. Bull.*, vol. 305, pp. 17–21, Jun. 2003.

[27] C. Cholachue, B. Ravelo, A. Simoens, A. Fathallah, M. Veronneau, and O. Maurice, "Braid shielding effectiveness Kron's Model via coupled cables configuration," *IEEE Trans. Circuits Syst. II, Exp. Briefs*, vol. 67, no. 8, pp. 1389–1393, Aug. 2020.

[28] C. Cholachue, B. Ravelo, A. Simoens, and A. Fathallah, "Fast S-parameter TAN model of n-port lumped structures," *IEEE Access*, vol. 7, pp. 72505–72517, 2019.